Inorganic Chemistry

Article

Single-Molecule Magnet Behavior in Heterometallic M^{II}–Mn^{III}_2–M^{II} Tetramers (M^{II} = Cu, Ni) Containing Mn^{III} Salen-Type Dinuclear Core

Chihiro Kachi-Terajima,[†,#] Hitoshi Miyasaka,*[,‡,⊥] Ayumi Saitoh,[†] Naoki Shirakawa,[§] Masahiro Yamashita,[‡,⊥] and Rodolphe Clérac[∥]

Department of Chemistry, Graduate School of Science, Tokyo Metropolitan University, 1-1 Minami-ohsawa, Hachioji, Tokyo 192-0397, Japan, Department of Chemistry, Graduate School of Science, Tohoku University, 6-3 Aramaki-Aza-Aoba, Aoba-ku, Sendai, Miyagi 980-8578, Japan, CREST, Japan Science and Technology Agency (JST), 4-1-8 Honcho, Kawaguchi, Saitama 332-0012, Japan, Nanoelectronics Research Institute, National Institute of Advanced Industrial Science and Technology (AIST), Umezono 1-1-1, Tsukuba, Ibaraki 305-8568, Japan, and Université Bordeaux 1, CNRS, Centre de Recherche Paul Pascal-UPR8641, 115 Avenue du Dr. A. Schweitzer, 33600 Pessac, France

The linear-type heterometallic tetramers, $[Mn^{III}_2(5\text{-MeOsaltmen})_2M^{II}_2(L)_2](CF_3SO_3)_2 \cdot 2H_2O$ (M^{II} = Cu, **1a**; Ni, **2a**), where 5-MeOsaltmen^{2-} = N,N'-(1,1,2,2-tetramethylethylene) bis(5-methoxysalicylideneiminate), and H_2L = 3-{2-[(2-hydroxy-benzylidene)-amino]-2-methyl-propylimino}-butan-2-one oxime, have been synthesized and characterized from structural and magnetic points of view. These two compounds are isostructural and crystallize in the same monoclinic $P2_1/n$ space group. The structure has a $[M^{II}\text{–NO–}Mn^{III}\text{–}(O)_2\text{–}Mn^{III}\text{–ON–}M^{II}]$ skeleton, where –NO– is a linking oximato group derived from the non-symmetrical Schiff-base complex $[M^{II}(L)]$ and –$(O)_2$– is a biphenolato bridge in the out-of-plane $[Mn_2(5\text{-MeOsaltmen})_2]^{2+}$ dimer. The solvent-free compounds, **1b** and **2b**, have also been prepared by drying of the parent compounds, **1a** and **2a**, respectively, at 100 °C under dried nitrogen. After this treatment, the crystallinity is preserved, and **1b** and **2b** crystallize in a monoclinic $P2_1/c$ space group without significant changes in their structures in comparison to **1a** and **2a**. Magnetic measurements on **1a** and **1b** revealed antiferromagnetic $Mn^{III}\cdots Cu^{II}$ interactions via the oximato group and weak ferromagnetic $Mn^{III}\cdots Mn^{III}$ interactions via the biphenolato bridge leading to an $S_T = 3$ ground state. On the other hand, the diamagnetic nature of the square planar Ni^{II} center generates an $S_T = 4$ ground state for **2a** and **2b**. At low temperature, these solvated (**a**) and desolvated (**b**) compounds display single-molecule magnet behavior modulated by their spin ground state.

Introduction

In recent years, the design of molecular superparamagnets called single-molecule magnets (SMMs)[1] has been an attractive research subject in the field of molecular magnetism.

The SMM property can be controlled by intrinsic properties of individual molecule, that is, high spin ground state (S_T) and uniaxial anisotropy (large negative D and small E considering the Hamiltonian anisotropy term $H = DS_{Tz}^2 + E(S_{Tx}^2 - S_{Ty}^2)$), that create a finite energy barrier (Δ) between the "spin-up" and "spin-down" m_s states ($m_s = \pm S_T$) expressed as $|D|S_T^2$ for integer S_T or $|D|(S_T^2 - 1/4)$ for half-integer S_T. One of the outstanding advantages of such molecular superparamagnets resides in their magnetic properties that are tunable by chemical treatments and modifications at the molecular level. So far, the common strategy to design SMM molecules relies mostly on the self-assembly of anisotropic metal ions such as high-spin Mn^{III} ion with appropriate magnetic mediators. Derived from this self-assembly approach, the design of new SMMs has also been

† Tokyo Metropolitan University.
‡ Tohoku University.
⊥ CREST-JST.
§ AIST.
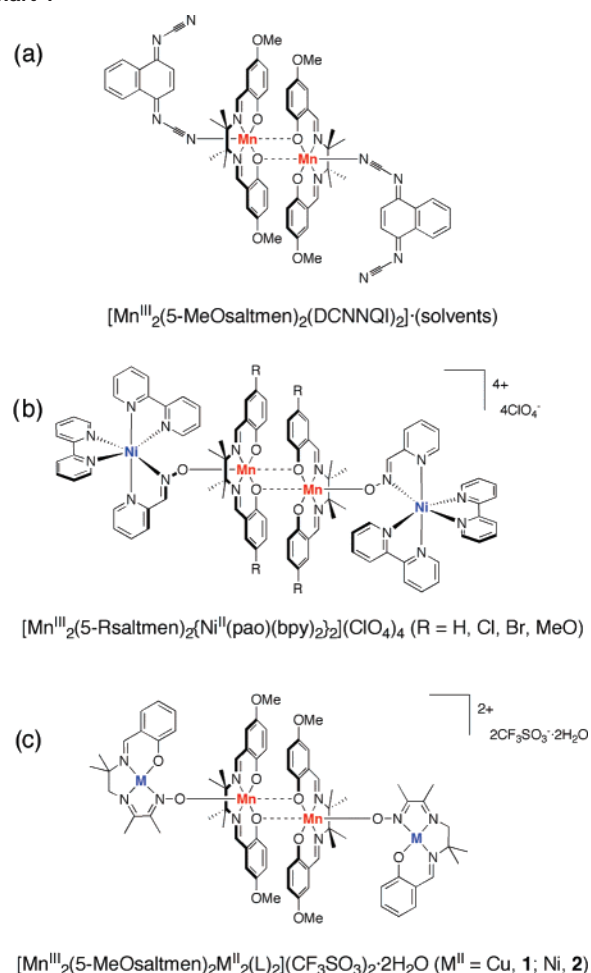∥ Université Bordeaux 1, Centre de Recherche Paul Pascal.
Current address: Department of Chemistry, Faculty of Science, Toho University, 2-2-1 Miyama, Funabashi, Chiba 274-8510, Japan.
(1) (a) Christou, G.; Gatteschi, D.; Hendrickson, D. N.; Sessoli, R. *MRS Bull.* **2000**, *25*, 66. (b) Gatteshi, D.; Sessoli, R. *Angew. Chem.* **2003**, *115*, 278; *Angew. Chem., Int. Ed.* **2003**, *42*, 268. (c) Gatteschi, D.; Sessoli, R.; Villain, J. *Molecular Nanomagnets*; Oxford University Press: Oxford, U.K., 2006.

achieved by chemical modification of the core structure of a known SMM to control its magnetic behavior and to evaluate the influence of the different chemical components. A few noteworthy examples, using this strategy, have been reported so far. Christou and Hendrickson et al. have been able to tune the magnetic properties and, especially, the energy barrier (Δ) in a redox series of Mn_{12} SMMs by electrochemical modification of a neutral parent Mn_{12} complex, $[Mn_{12}O_{12}(O_2R)_{16}(H_2O)_4]$ ($S_T = 10$), to a one-electron reduced form, $[Mn_{12}O_{12}(O_2R)_{16}(H_2O)_4]^-$ ($S_T = 19/2$), and a two-electron reduced form, $[Mn_{12}O_{12}(O_2R)_{16}(H_2O)_4]^{2-}$ ($S_T = 10$) (O_2R = carboxylato). They found that the energy barrier of these redox compounds changed dramatically upon their oxidation state: $\Delta_{[Mn_{12}]^0} > \Delta_{[Mn_{12}]^-} > \Delta_{[Mn_{12}]^{2-}}$.[2] They also characterized two Jahn−Teller isomers of $[Mn_{12}O_{12}(O_2CCH_2$-$Bu^t)_{16}(H_2O)_4]·(S)$ that exhibit different SMM properties modulated by the interstitial solvents, S.[3] Another example was given by Awaga et al. who succeeded in substituting one Mn^{III} center of a Mn_{12} cluster with a Cr^{III} ion, $[Mn_{11}CrO_{12}(O_2CCH_3)_{16}(H_2O)_4]·2CH_3CO_2H·4H_2O$. This new complex exhibits SMM properties but is clearly different from the original Mn_{12} SMM cluster.[4]

Recently, our group has reported two Mn^{III} salen-type out-of-plane dimeric complexes decorated by an organic radical, N,N'-dicyano-1,4-naphthoquinonediiminate (DCNNQI•−), with different interstitial solvents, $[Mn_2(5\text{-MeOsaltmen})_2$-$(DCNNQI)_2]·(S)$ (with 5-MeOsaltmen^{2-} = N,N'-(1,1,2,2-tetramethylethylene) bis(5-MeOsalicylideneiminate) and S = MeOH or $2CH_2Cl_2·2CH_3CN$; Chart 1a).[5] The magnetic properties of these compounds are strongly dependent on their crystal packing. Indeed, while the complex with S = MeOH is a SMM with an $S_T = 3$ ground state, the complex with S = $2CH_2Cl_2·2CH_3CN$ possesses a diamagnetic ground state because of a strong antiferromagnetic coupling between the Mn^{III} centers through space and through the $(DCNNQI)_2$ diamagnetic dimers. Thus, an important part of our research activity has been devoted to the synthesis and chemical tuning of a SMM series built on the Mn^{III} saltmen out-of-plane dimeric complexes, $[Mn_2(5\text{-Rsaltmen})_2(L)_2]^{n+}$,[6] where L is an axially coordinating organic or inorganic ligand like DCNNQI in the above example (Chart 1a) or a complex with

Chart 1

(a)

$[Mn^{III}_2(5\text{-MeOsaltmen})_2(DCNNQI)_2]·(\text{solvents})$

(b)

$[Mn^{III}_2(5\text{-Rsaltmen})_2\{Ni^{II}(pao)(bpy)_2\}_2](ClO_4)_4$ (R = H, Cl, Br, MeO)

(c)

$[Mn^{III}_2(5\text{-MeOsaltmen})_2M^{II}_2(L)_2](CF_3SO_3)_2·2H_2O$ (M^{II} = Cu, **1**; Ni, **2**)

a coordination-donor character (coordination-donor building block) like $[Ni(pao)(bpy)_2]^+$ (pao$^-$ = pyridine-2-aldoximate, bpy = 2,2'-bipyridine) (Chart 1b). In this vein, our research strategy has been oriented toward the use of monodentate coordination-donor building blocks (ML) to form linear-type $[Mn_2(5\text{-Rsaltmen})_2(ML)_2]^{n+}$ tetranuclear complexes with a $[M−Mn^{III}−Mn^{III}−M]$ metal arrangement. Interestingly, this approach allows to fine-tune of the magnetic properties (and the possible SMM behavior) of the resulting complexes, and in particular, to control the change of their spin ground state depending on the nature of the ML group. A series of linear-type tetranuclear compounds, $[Mn_2(5\text{-Rsaltmen})_2\{Ni$-$(pao)(bpy)_2\}_2](ClO_4)_4$ (R = H, Cl, Br, MeO), have already been obtained using $[Ni(pao)(bpy)_2]^+$ (Chart 1b).[7] Unfortunately, these compounds, which possess an $S_T = 2$ ground state, are not SMMs above 1.8 K.

In the present work, we focus on coordination-donor building blocks based on 3-{2-[(2-hydroxo-benzylidene)-amino]-2-methyl-propylimino}-butan-2-one oximato (L^{2-}). Costes et al. was the first to report on this type of complexes (with M = Cu^{II}) that act as bidentate units when assembled with lanthanide metal ions (in μ-phenolato- μ-oximato fashion).[8] We show that this type of building block can also

(2) (a) Eppley, H. J.; Tsai, H.-L.; Vries, N.; Folting, K.; Christou, G.; Hendrickson, D. N. *J. Am. Chem. Soc.* **1995**, *117*, 301. (b) Aubin, S. M. J.; Sun, Z.; Pardi, L.; Krzystek, J.; Folting, K.; Brunel, L.-C.; Rheingold, A. L.; Christou, G.; Hendrickson, D. N. *Inorg. Chem.* **1999**, *38*, 5329. (c) Soler, M.; Chandra, S. K.; Ruiz, D.; Davidson, E. R.; Hendrickson, D. N.; Christou, G. *Chem. Commun.* **2000**, 2417. (d) Soler, M.; Chandra, S. K.; Ruiz, D.; Huffman, J. C.; Hendrickson, D. N.; Christou, G. *Polyhedron* **2001**, *20*, 1279. (e) Soler, M.; Wernsdorfer, W.; Abboud, K. A.; Hendrickson, D. N.; Christou, G. *Polyhedron* **2003**, *22*, 1777. (f) Kuroda-Sowa, T.; Nogami, T.; Konaka, H.; Maekawa, M.; Munakata, M.; Miyasaka, H.; Yamashita, M. *Polyhedron* **2003**, *22*, 1795. (g) Soler, M.; Wernsdorfer, W.; Abboud, K. A.; Huffman, J. C.; Davidson, E. R.; Hendrickson, D. N.; Christou, G. *J. Am. Chem. Soc.* **2003**, *125*, 3576.

(3) Soler, M.; Wernsdorfer, W.; Sun, Z.; Huffman, J. C.; Hendrickson, D. N.; Christou, G. *Chem. Commun.* **2003**, *21*, 2672.

(4) Hachisuka, H.; Awaga, K.; Yokoyama, T.; Kubo, T.; Goto, T.; Nojiri, H. *Phys. Rev. B* **2004**, *70*, 104427.

(5) Kachi-Terajima, C.; Miyasaka, H.; Sugiura, K.-i.; Clérac, R.; Nojiri, H. *Inorg. Chem.* **2006**, *45*, 4381.

(6) Miyasaka, H.; Clérac, R.; Wernsdorfer, W.; Lecren, L.; Bonhomme, C.; Sugiura, K.-i.; Yamashita, M. *Angew. Chem., Int. Ed.* **2004**, *43*, 2801.

(7) Miyasaka, H.; Nezu, T.; Sugimoto, K.; Sugiura, K.-i.; Yamashita, M.; Clérac, R. *Inorg. Chem.* **2004**, *43*, 5486.

act as a monodentate coordinating unit using only the oximato coordination-donor site when assembled to $[Mn_2-(5\text{-Rsaltmen})_2]^{2+}$ cations. With $M^{II} = Cu^{II}$ and Ni^{II}, isostructural linear-type tetranuclear compounds, $[Mn_2(5\text{-MeOsaltmen})_2M_2(L)_2](CF_3SO_3)_2 \cdot 2H_2O$ (M = Cu (**1a**), Ni (**2a**)) (Chart 1c), have been synthesized and their desolvated compounds (**1b** and **2b**) have also been prepared by drying **1a** and **2a** at 100 °C. These compounds have a common $[M^{II}-NO-Mn^{III}-(O_{Ph})_2-Mn^{III}-ON-M^{II}]$ bridging skeleton. Depending on the spin state of the M^{II} ion ($S_{Cu} = 1/2$, $S_{Ni} = 0$) and on different exchange couplings mediated by the $M^{II}-NO-Mn^{III}$ and $Mn^{III}-(O_{Ph})_2-Mn^{III}$ bridges, the ground state of **1** (**1a** and **1b**) and **2** (**2a** and **2b**) are $S_T = 3$ and $S_T = 4$, respectively. As we will show, all these compounds exhibit SMM properties that are tuned by the choice of the M^{II} ions independently of the presence or absence of interstitial solvents.

Experimental Section

General Procedures and Materials. All chemicals and solvents used during the syntheses were reagent grade. Solvents for syntheses of **1a** and **2a** were initially used without specific treatments. The starting material $[Mn_2(5\text{-MeOsaltmen})_2(H_2O)_2](CF_3SO_3)_2$ was prepared following the reported method.[9] The complex [Cu(L)] was prepared according to the method in the literature,[8] and [Ni(L)] was synthesized in a similar way.

$[Mn_2(5\text{-MeOsaltmen})_2Cu_2(L)_2](CF_3SO_3)_2 \cdot 2H_2O$ (1a). An ethanol solution (40 mL) of $[Mn_2(5\text{-MeOsaltmen})_2(H_2O)_2](CF_3SO_3)_2$ (0.060 g, 0.050 mmol) was added to an ethanol solution (25 mL) of [Cu(L)] (0.032 g, 0.095 mmol). After the mixture was stirred for 10 min, 10 mL of water was added, and then the mixture was filtered. The resulting filtrate was left undisturbed for 2 weeks to form dark brown block crystals of **1a**. Yield: 40% (based on Mn ion). Anal. Calcd for $C_{76}H_{94}N_{10}O_{20}Cu_2F_6Mn_2S_2$: C, 48.48; H, 5.03; N, 7.44. Found: C, 48.47; H, 4.91; N, 7.26. IR (cm^{-1}) (KBr): ν(C=N) 1622, 1601; ν(CF$_3$SO$_3^-$) 1279, 1227, 1030, 638.

$[Mn_2(5\text{-MeOsaltmen})_2Cu_2(L)_2](CF_3SO_3)_2$ (1b). Thermogravimetric (TG) measurements were performed to prepare the solvent-free sample of **1a** in a controlled manner. Crystals of **1a** were heated from room temperature to 100 °C at a heating rate 5 °C/min, then kept for 20 min at 100 °C, and finally cooled to room temperature under flowing dried nitrogen to obtain crystals of **1b**. The crystallization solvents (two H$_2$O molecules) of **1a** were removed completely when the temperature was increased up to 100 °C. The total mass loss is 1.45% (calcd 1.91%). Anal. Calcd for $C_{76}H_{90}N_{10}O_{18}Cu_2F_6Mn_2S_2$: C, 49.43; H, 4.91; N, 7.58. Found: C, 49.44; H, 5.00; N, 7.49. IR (cm^{-1}) (KBr): ν(C=N) 1622, 1601; ν(CF$_3$SO$_3^-$) 1279, 1227, 1030, 638.

$[Mn_2(5\text{-MeOsaltmen})_2Ni_2(L)_2](CF_3SO_3)_2 \cdot 2H_2O$ (2a). The synthetic procedure for **2a** was almost identical for **1a**. An ethanol/methanol (1:1) solution containing [Ni(L)] was used instead of the ethanol solution of [Cu(L)]. Yield: 71% (based on Mn ion). Anal. Calcd for $C_{76}H_{94}N_{10}O_{20}Ni_2F_6Mn_2S_2$: C, 48.74; H, 5.06; N, 7.48. Found: C, 48.58; H, 4.99; N, 7.50. IR (cm^{-1}) (KBr): ν(C=N) 1612, 1601; ν(CF$_3$SO$_3^-$), 1281, 1227, 1030, 638.

$[Mn_2(5\text{-MeOsaltmen})_2Ni_2(L)_2](CF_3SO_3)_2$ (2b). Compound **2b** was obtained with the same experimental procedure as **1b**. The total mass loss is 1.83% (calcd 1.92%). Anal. Calcd for $C_{76}H_{90}N_{10}O_{18}Ni_2F_6Mn_2S_2$: C, 49.69; H, 4.94; N, 7.62. Found: C, 49.47; H, 4.85; N, 7.61. IR (cm^{-1}) (KBr): ν(C=N) 1614, 1601; ν(CF$_3$SO$_3^-$) 1277, 1229, 1032, 638.

Physical Measurements. Infrared spectra were measured on KBr disks with a Shimadzu FT-IR-8600 spectrophotometer. Thermogravimetric (TG) analysis and differential thermal analysis (DTA) for preparing **1b** and **2b** were carried out using a RIGAKU Thermo Plus TG-8120 apparatus with a heating/cooling rate of 5 °C/min in flowing dried N$_2$. The magnetic susceptibility measurements were conducted with the use of a Quantum Design SQUID magnetometer (MPMS-XL) in the temperature and dc field ranges of 1.8 to 300 K and -7 to 7 T, respectively; ac measurements were performed at various frequencies from 1 to 1488 Hz with ac field amplitude of 3 Oe. Experimental data were corrected for the sample holder and for the diamagnetic contribution calculated from Pascal constants.[10] The polycrystalline samples were also measured by restraining in *n*-eicosane matrix and after correction of this additional diamagnetic contribution, no significant change in the magnetic behavior has been observed. The magnetizations on a single crystal below 1.8 K were measured with a Quantum Design SQUID magnetometer MPMS attaching a ^{3}He refrigerator (IQUANTUM iHelium3) applying up to ± 1 T external field. The crystal lattice orientation of the used single crystal was first determined by X-ray crystallography using a RIGAKU four-axis diffractometer (AFC7R) and CCD diffractometer (Saturn70), and the crystal (0.8 $\times$ 1.8 $\times$ 2.0 mm^3) was placed in a SQUID gelatin capsule with N-Apiezon grease. The single-crystal preoriented by X-ray diffraction can still move in the viscous grease even at 300 K when high fields are applied. Therefore, by application of 7 T at this temperature, the crystal orientation was adjusted in its easy magnetization direction. This orientation was then frozen by decreasing the temperature below the solidification temperature of the grease.

Crystallography. Single crystals with dimensions of 0.25 $\times$ 0.25 $\times$ 0.15 mm^3 for **1a**, 0.25 $\times$ 0.25 $\times$ 0.10 mm^3 for **1b**, 0.25 $\times$ 0.25 $\times$ 0.20 mm^3 for **2a**, and 0.20 $\times$ 0.20 $\times$ 0.10 mm^3 for **2b** were mounted on a glass rod. Data collections were made on a Rigaku CCD diffractometer (Saturn70) with a graphite-monochromated Mo Kα radiation ($\lambda = 0.71070$ Å). The structures were solved by direct methods (SIR92)[11] and expanded using Fourier techniques (DIRDIF99).[12] The non-hydrogen atoms were refined anisotropically. Hydrogen atoms were refined using the riding model. The final cycle of full-matrix least-squares refinements on F^2 was based on observed reflections and variable parameters and converged with unweighted and weighted agreement factors of R1 = $\sum||F_o| - |F_c||/\sum|F_o|$ ($I > 2.00\sigma(I)$) and wR2 = $[\sum w(F_o^2 - F_c^2)^2/\sum w(F_o^2)^2]^{1/2}$ (all data). A Sheldrick weighting scheme was used. Neutral atom scattering factors were taken from Cromer and Waber.[13] Anomalous dispersion effects were included in F_{calcd}; the values $\Delta f'$ and $\Delta f''$

(8) (a) Costes, J. P.; Dahan, F.; Dupuis, A.; Laurent, J. P. *New J. Chem.* **1997**, *21*, 1211. (b) Costes, J. P.; Dahan, F.; Dupuis, A.; Laurent, J. P. *J. Chem. Soc., Dalton Trans.* **1998**, 1307. (c) Costes, J. P.; Dahan, F.; Dupuis, A.; Laurent, J. P. *Inorg. Chem.* **2000**, *39*, 169. (d) Costes, J. P.; Dahan, F.; Dupuis, A. *Inorg. Chem.* **2000**, *39*, 5994.

(9) Miyasaka, H.; Clérac, R.; Ishii, T.; Chang, H.-C.; Kitagawa, S.; Yamashita, M. *J. Chem. Soc., Dalton Trans.* **2002**, 1528.

(10) Boudreaux, E. A.; Mulay, L. N. *Theory and Applications of Molecular Paramagnetism*; John Wiley and Sons: New York, 1976; pp 491−495.

(11) SIR92: Altomare, A.; Cascarano, G.; Giacovazzo, C.; Guagliardi, A.; Burla, M.; Polidori, G.; Camalli, M. *J. Appl. Crystallogr.* **1994**, *27*, 435.

(12) DIRDIF99: Beurskens, P. T.; Admiraal, G.; Beurskens, G.; Bosman, W. P.; de Gelder, R.; Israel, R.; Smits, J. M. M. *The DIRDIF-99 Program System*; Technical Report of the Crystallography Laboratory; University of Nijmegen: Nijmegen, The Netherlands, 1999.

(13) Cromer, D. T.; Waber, J. T. *International Tables for Crystallography*; The Kynoch Press: Birmingham, England, 1974; Vol IV, Table 2.2A.

Table 1. Crystallographic Data for **1a**, **1b**, **2a**, and **2b**

compound	1a	1b	2a	2b
formula	$C_{76}H_{94}N_{10}O_{20}Cu_2F_6Mn_2S_2$	$C_{76}H_{90}N_{10}O_{18}Cu_2F_6Mn_2S_2$	$C_{76}H_{94}N_{10}O_{20}Ni_2F_6Mn_2S_2$	$C_{76}H_{90}N_{10}O_{18}Ni_2F_6Mn_2S_2$
fw	1882.71	1846.68	1873.02	1836.99
cryst syst	monoclinic	monoclinic	monoclinic	monoclinic
space group	$P2_1/n$ (No. 14)	$P2_1/c$ (No. 14)	$P2_1/n$ (No. 14)	$P2_1/c$ (No. 14)
λ(Mo Kα) (Å)	0.71070	0.71070	0.71070	0.71070
a (Å)	17.078(7)	16.839(7)	16.853(6)	16.645(9)
b (Å)	11.888(4)	12.120(5)	11.904(4)	12.098(6)
c (Å)	21.335(9)	20.886(9)	21.360(7)	20.738(11)
β (deg)	113.1168(11)	113.4930(15)	113.1311(11)	112.6685(14)
V (Å^3)	3984(3)	3909(3)	3941(2)	3853(3)
Z	2	2	2	2
T (K)	103 ± 1	103 ± 1	103 ± 1	103 ± 1
μ(Mo Kα) (cm^{-1})	9.814	9.967	9.303	9.479
D_{calcd} (g cm^{-3})	1.569	1.569	1.578	1.583
F_{000}	1948.00	1908.00	1944.00	1904.00
$2\theta_{max}$ (deg)	62.1	62.0	61.9	62.2
reflns measured	35 248	33 217	34 815	34 568
reflns used	6745	8911	8786	8820
params	577	568	577	568
R1 [$I > 2\sigma(I)$]^a	0.0698	0.0652	0.0443	0.0537
wR2 [all data]^b	0.2016	0.1865	0.1367	0.1421
GOF on F^2	1.179	1.060	1.090	1.014
ρ_{max}/ρ_{min} (e$^-$ Å^{-3})	2.03/−1.24	2.15/−1.03	0.91/−0.81	1.40/−0.77

^{a} R1 = $\sum||F_o| - |F_c||/\sum|F_o|$ ($I > 2.00\sigma(I)$). ^{b} wR2 = $[\sum w(F_o^2 - F_c^2)^2/\sum w(F_o^2)^2]^{1/2}$ (all data).

Scheme 1
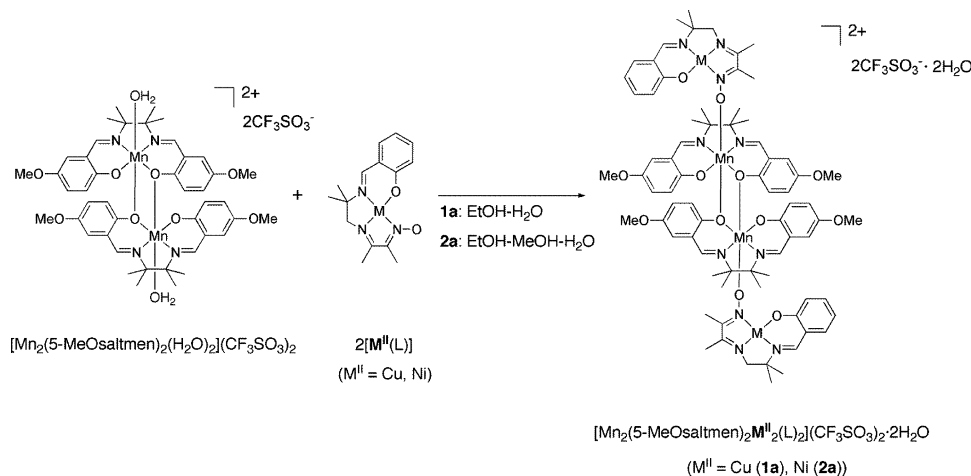
were those of Creagh and McAuley.[14] The values for the mass attenuation coefficients are those of Creagh and Hubbell.[15] All calculations were performed using the CrystalStructure crystallographic software package.[16] The detail of crystallographic data for **1a**, **1b**, **2a**, and **2b** are listed in Table 1.

Results and Discussion

Syntheses. The assembly reaction of [Mn$_2$(5-MeOsaltmen)$_2$-(H$_2$O)$_2$](CF$_3$SO$_3$)$_2$ and [M^{II}(L)] (M^{II} = Cu, Ni) in an ethanol/H$_2$O solution for M^{II} = Cu and an ethanol/methanol/H$_2$O solution for M^{II} = Ni yields large crystals (∼2 mm) of heterometallic linear complexes of **1a** and **2a**, respectively (Scheme 1). Both compounds **1a** and **2a** contain two interstitial H$_2$O molecules that are gradually eliminated by

heating and completely removed at 100 °C, followed by decomposition of **1a** and **2a** with the abrupt loss of weight at around 200 °C as seen in Figure 1. After the elimination of the interstitial water molecules and before decomposition, the desolvated compounds, called **1b** and **2b** hereafter, retain their crystallinity, and single-crystal X-ray diffraction analysis can still be performed (vide infra). Therefore, the samples of **1b** and **2b** for X-ray crystallography and magnetic measurements were prepared by the following procedures: heating crystals of **1a** and **2a**, respectively, from room temperature to 100 °C at a heating rate of 5 °C/min, holding for 20 min at 100 °C, and finally cooling to room temperature under dried nitrogen flow.

Structural Description. Compounds **1a** and **2a** and their desolvated compounds **1b** and **2b** are quasi-isostructural and crystallize in the monoclinic $P2_1/n$ (No. 14) for **1a** and **2a** and $P2_1/c$ (No. 14) for **1b** and **2b** with very similar cell dimensions. ORTEP drawings of the cationic part of **1a** and **2a** are depicted in Figure 2 (ORTEPs of **1b** and **2b** are depicted in Figure S1). Relevant bond distances and angles

(14) Creagh, D. C.; McAuley, W. J. In *International Tables for Crystallography*; Wilson, A. J. C., Ed.; Kluwer Academic Publishers: Boston, 1992; Vol C, Table 4.2.6.8, pp 219−222.

(15) Creagh, D. C.; Hubbell, J. H. In *International Tables for Crystallography*; Wilson, A. J. C., Ed.; Kluwer Academic Publishers: Boston, 1992; Vol C, Table 4.2.4.3, pp 200−206.

(16) *CrystalStructure 3.15: Crystal Structure Analysis Package*; Rigaku and Rigaku/MSC9009: The Woodlands, TX, 2000−2002.
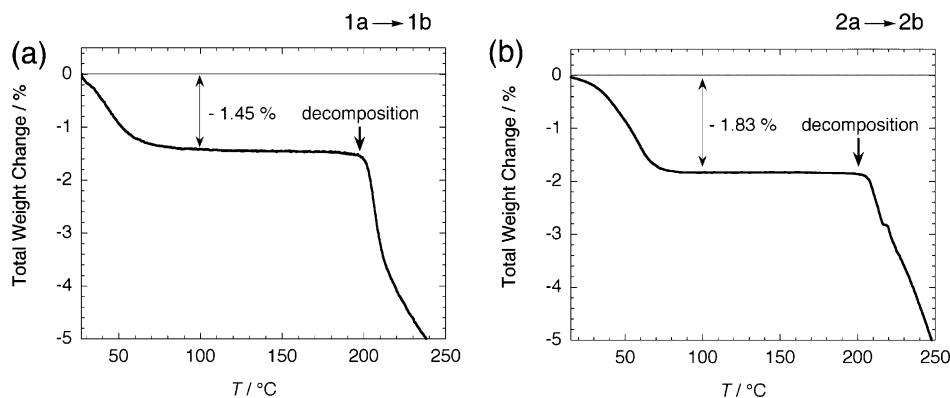
Figure 1. Thermogravimetric (TG) curves of **1a** (a) and **2a** (b). The heating rate was 5 °C/min in a dried nitrogen stream.
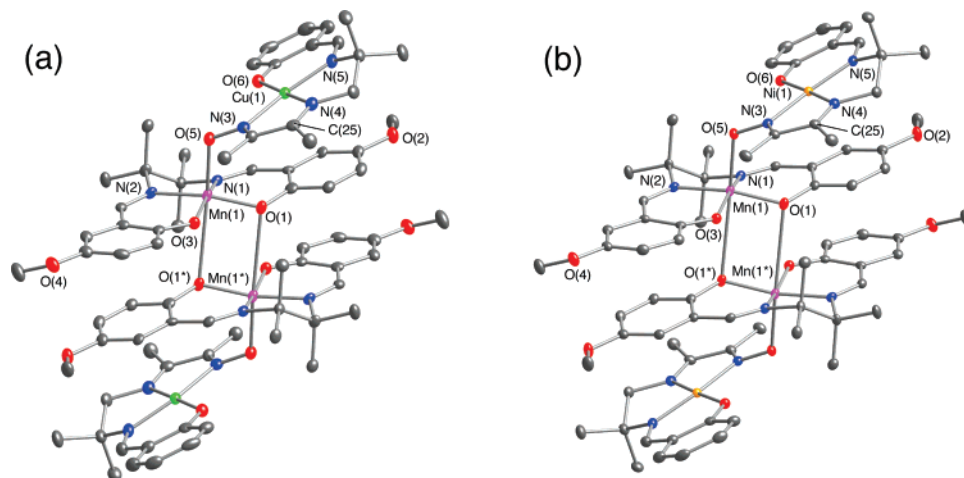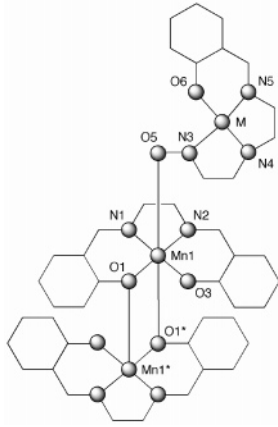

Figure 2. ORTEP drawings of the cationic part of **1a** (a) and **2a** (b) with thermal ellipsoids at 50% probability. Hydrogen atoms are omitted for clarity.

are summarized in Table 2. All compounds have a [M^{II}–NO–Mn^{III}–$(O_{Ph})_2$–Mn^{III}–ON–M^{II}] bridging skeleton with an inversion center in the midpoint of Mn–$(O_{Ph})_2$–Mn moiety (where –NO– is an oximato bridge coming from the [M(L)] moiety and –$(O_{Ph})_2$– is a biphenolato bridge in the [Mn_2(5-MeOsaltmen)$_2$]$^{2+}$ dimeric moiety). This bridging motif is similar to the previously reported compounds, [Mn_2-(5-Rsaltmen)$_2${Ni(pao)(bpy)$_2$}](ClO$_4$)$_4$ (Chart 1b).[7] In the present four compounds, the M^{II} metal ion has a slightly distorted square planar coordination geometry surrounded by three nitrogen atoms and one oxygen atoms with bond distances of M–O(6) = 1.876(3) Å for **1a**, 1.872(2) Å for **1b**, 1.8269(18) Å for **2a**, and 1.8244(19) Å for **2b**, and $<M–N>_{av}$ = 1.963 Å for **1a**, 1.957 Å for **1b**, 1.861 Å for **2a**, and 1.859 Å for **2b**. As expected, the oxygen atom O(5) of the oximato function does not chelate to the M^{II} site but acts as a bridging group between the M^{II} and Mn^{III} ions in a M^{II}–NO–Mn^{III} fashion (i.e., the [M^{II}(L)] moiety is acting as a monodentate coordination-donor building block). The "heart" of these tetranuclear complexes is made of the Mn–$(O_{Ph})_2$–Mn core that is very similar to those observed in [Mn_2-(saltmen)$_2$(H$_2$O)$_2$](ClO$_4$)$_2$ and its derivatives.[5,6,7,9,17] Each Mn^{III} ion is equatorially surrounded by N$_2$O$_2$ atoms of the 5-MeOsaltmen^{2-} quadridentate Schiff-base ligand with average bond distances of $<Mn–N>_{av}$ = 1.995 Å for **1a**, 1.993 Å for **1b**, 1.989 Å for **2a**, and 1.989 Å for **2b**, and $<Mn–O>_{av}$ = 1.877 Å for **1a**, 1.876 Å for **1b**, 1.872 Å for **2a**,

and 1.877 Å for **2b**. One of the Mn^{III} apical positions is occupied by the phenolato oxygen O(1)* from the neighboring [Mn(5-MeOsaltmen)]$^+$ moiety with the following distances and angles in the bridging core: Mn(1)–O(1)* = 3.081(2) Å for **1a**, 2.858(2) Å for **1b**, 3.1132(14) Å for **2a**, 2.842(2) Å for **2b**; O(1)–Mn(1)–O(1)* = 85.11(11)° for **1a**, 82.58(9)° for **1b**, 84.04(5)° for **2a**, 81.48(8)° for **2b**; Mn-(1)–O(1)–Mn(1)* = 94.89(12)° for **1a**, 97.42(10)° for **1b**, 95.96(6)° for **2a**, 98.52(9)° for **2b** [symmetry operation $-x$ + 2, $-y$, $-z$ + 2 for **1a** and **2a**; $-x$ + 1, $-y$, $-z$ + 1 for **1b** and **2b**]. It is interesting to note that the Mn–O(1)* bond distance in the desolvated compounds is significantly shorter than in the solvated compounds (indeed more than 0.22 Å shorter), and furthermore, the O(1)–Mn(1)-O(1)* and Mn-(1)–O(1)-Mn(1)* angles in the desolvated compounds become, respectively, smaller and bigger than in the solvated compounds (consequently, with the removal of the solvent molecules, the out-of-plane Mn^{III} dinuclear core is squashed in the axial direction and slipped in the in-plane direction). The oximato function of the [M^{II}(L)] moiety coordinates to each apical position of the [Mn_2(5-MeOsaltmen)$_2$]$^{2+}$ dimeric moiety with bond distances and angles of Mn(1)–O(5) = 2.104(3) Å for **1a**, 2.109(2) Å for **1b**, 2.1093(16) Å for **2a**, 2.123(2) Å for **2b**; and Mn(1)–O(5)-N(3) = 117.6(2)° for **1a**, 117.45(18)° for **1b**, 118.55(13)° for **2a**, 118.69(16)° for **2b**. The axial bond distances are significantly longer than the equatorial ones as expected for semicoordinating ligands

Table 2. Relevant Bond Distances (Å) and Angles (deg) Around the Coordinated Metal Ions for **1a**, **2a**, **1b**, and **2b** with the Estimated Standard Deviations in Parentheses

	1a	**1b**	**2a**	**2b**
Mn1−O1	1.879(3)	1.876(2)	1.8715(19)	1.8765(19)
Mn1−O3	1.875(2)	1.876(2)	1.8720(14)	1.878(2)
Mn1−N1	1.999(3)	2.008(2)	1.9953(17)	1.995(2)
Mn1−N2	1.990(4)	1.977(2)	1.982(2)	1.982(2)
Mn1−O5	2.104(3)	2.109(2)	2.1093(16)	2.123(2)
Mn1−O1^a	3.081(2)	2.858(2)	3.1132(14)	2.842(2)
Mn1···Mn1^a	3.7436(8)	3.6157(6)	3.7953(5)	3.6305(6)
M1^b−N3	2.006(3)	1.996(2)	1.8993(18)	1.895(3)
M1^b−N4	1.938(4)	1.934(2)	1.832(2)	1.833(2)
M1^b−N5	1.945(4)	1.942(3)	1.853(2)	1.848(3)
M1^b−O6	1.876(3)	1.872(2)	1.8269(18)	1.8244(19)
O1−Mn1−O3	90.12(13)	91.03(10)	90.21(7)	91.31(9)
O1−Mn1−N1	91.72(14)	91.47(10)	91.58(7)	91.71(9)
O1−Mn1−N2	166.60(13)	166.74(11)	166.44(7)	166.65(10)
O1−Mn1−O5	95.84(14)	95.24(9)	95.57(7)	94.66(9)
O1−Mn1−O1^a	85.11(11)	82.58(9)	84.04(5)	81.48(8)
O3−Mn1−N1	164.01(13)	166.22(12)	163.25(7)	166.18(11)
O3−Mn1−N2	92.80(14)	93.38(11)	92.29(7)	92.73(10)
O3−Mn1−O5	95.66(11)	93.57(10)	96.50(6)	93.98(9)
O3−Mn1−O1^a	72.40(10)	75.39(9)	72.05(5)	75.63(8)
N1−Mn1−N2	81.95(14)	81.38(11)	82.26(8)	81.48(10)
N1−Mn1−O5	99.95(12)	99.69(11)	99.90(6)	99.21(10)
N1−Mn1−O1^a	91.93(10)	91.50(10)	91.57(5)	91.49(9)
N2−Mn1−O5	96.87(14)	96.96(10)	97.38(7)	97.74(9)
N2−Mn1−O1^a	83.32(11)	86.43(9)	84.07(6)	87.21(9)
O5−Mn1−O1^a	168.04(9)	168.66(8)	168.53(5)	168.76(7)
Mn1−O1−Mn1^a	94.89(12)	97.42(10)	95.96(6)	98.52(9)
Mn1−O5−N3	117.6(2)	117.45(18)	118.55(13)	118.69(16)
M1^b−N3−O5	126.4(2)	126.1(2)	125.77(13)	125.6(2)
N3−M1^b−N4	80.72(16)	81.18(12)	82.93(9)	83.14(12)
N3−M1^b−N5	164.13(17)	164.64(10)	168.66(9)	169.06(10)
N3−M1^b−O6	99.27(15)	98.89(11)	94.44(8)	94.04(11)
N4−M1^b−N5	83.51(16)	83.49(12)	85.90(9)	85.97(13)
N4−M1^b−O6	178.23(13)	177.05(11)	177.37(8)	177.11(13)
N5−M1^b−O6	96.44(15)	96.39(11)	96.73(8)	96.83(11)

^{a} Symmetry operations: $-x + 2, -y, -z + 2$ for **1a** and **2a**; $-x + 1, -y, -z + 1$ for **1b** and **2b**. ^{b} M1 = Cu for **1a**, **1b**; Ni for **2a**, **2b**.

and Jahn−Teller distortion of Mn^{III} ions. While the Mn^{III}_2 core is sensitive to the loss of the interstitial water molecules, the $M^{II}-NO-Mn^{III}$ bridges stay almost unchanged. Thus, the dihedral angle between the equatorial $Mn-N_2O_2$ plane and the average $M-N_3O_2$ plane is almost the same through all the series: 27.650° for **1a**, 27.731° for **1b**, 28.009° for **2a**, and 27.769° for **2b**. Therefore, the elimination of the interstitial solvents influenced almost exclusively the Mn^{III} dinuclear unit geometry of these complexes.
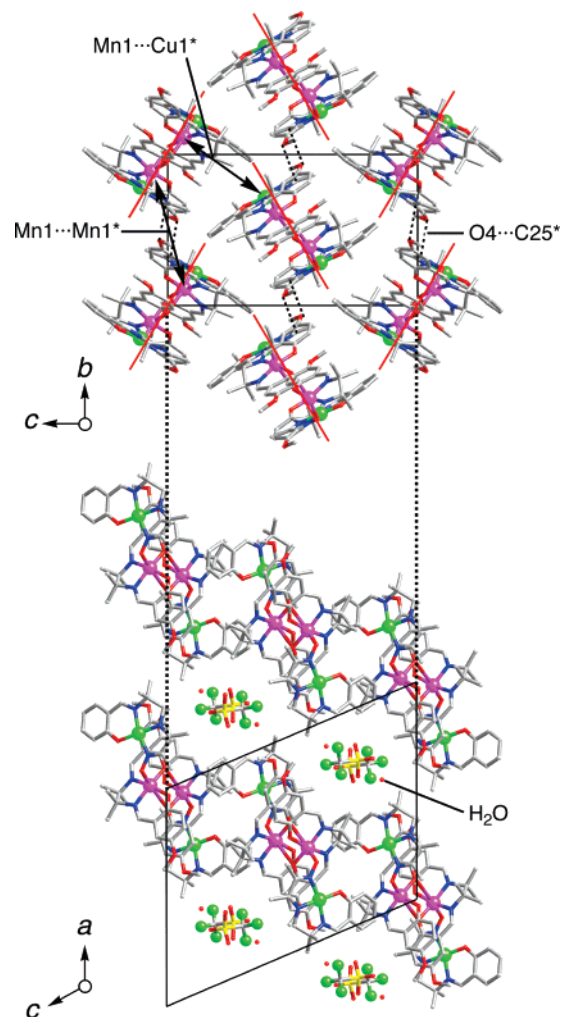
Figure 3. Packing diagram of **1a** showing the projection along the a-axis (top) and b-axis (bottom), where the red line represents the expected magnetic easy-axis direction for each molecule. The intermolecular shortest contact is found in O(4)···C(25)*, displayed as a dashed line (see text).

All these tetranuclear complexes possess a very similar packing arrangement. Therefore, **1a** is shown in Figure 3 as a representative illustration. The molecules lie in the (1, 0, −1) plane for **1a** (Figure 3a) and **2a** and the (1, 0, 0) plane for **1b** (Figure S2) and **2b**, forming a pseudolayer that alternates with the $CF_3SO_3^-$ anion layers along the a-axis (note that for **1a** and **2a**, interstitial water molecules are joining the counteranion layer as shown in Figure 3b, where the water molecules (O(10)) form a hydrogen bond with one of the oxygen atoms of $CF_3SO_3^-$ at 2.970(7) Å for **1a** and 2.940(3) Å for **2a**). Within the cationic layer, two molecular orientations of the tetranuclear complex are found with an angle of 65° (Figure 3a). It is worth noting that there is no significant direct contact between complexes such as hydrogen bonding or $\pi-\pi$ stacking between the molecules, but the closest intermolecular distance located between O(4) of the 5-MeOsaltmen^{2-} ligand and C(25)* of the [M^{II}(L)] moiety positioned in $(-x + 2, -y + 1, -z + 2)$ for **1a** and **2a** and $(-x + 1, -y + 1, -z + 1)$ for **1b** and **2b** are relatively short with 3.239(5) Å for **1a**, 3.239(4) Å for **1b**, 3.209(2) Å for **2a**, and 3.210(4) Å for **2b** (dashed black lines in Figure 3a). The intermolecular nearest metal···metal
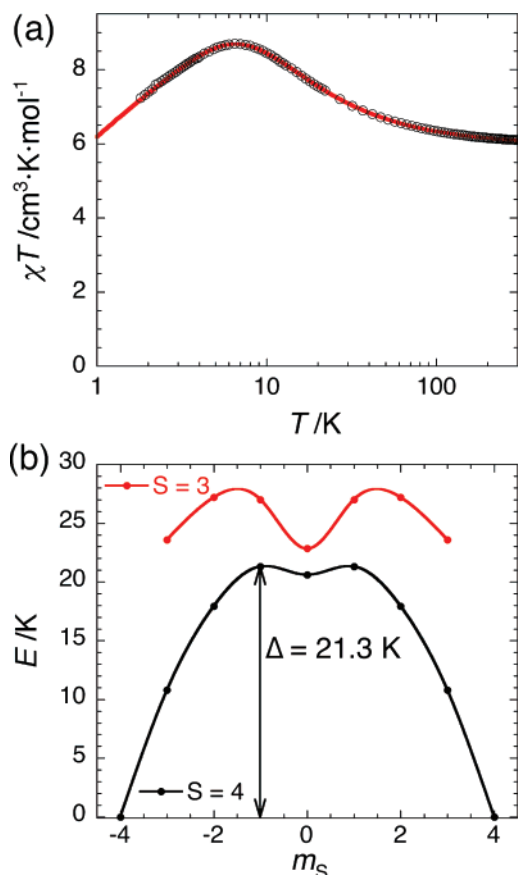
Figure 4. (a) Plots of χT vs T for **2a** at 1 kOe. The solid red line represents best-fit curve obtained with a dinuclear $Mn^{III}-Mn^{III}$ model (see text). (b) Energy diagram of the two lowest spin states calculated from the fitting parameters of the χT vs T data. Note that only the dominant spin contribution for each state was kept to make this figure.

distance is found between Mn^{III} and M^{II} in the *bc* plane: 7.9265(7) Å for **1a** ($Mn\cdots Cu^*$), 7.8702(5) Å for **1b** ($Mn\cdots Cu^*$), 7.9461(4) Å for **2a** ($Mn\cdots Ni^*$), and 7.8801(5) Å for **2b** ($Mn\cdots Ni^*$) (symmetry operations (*) $-x + 3/2$, $y - 1/2$, $-z + 3/2$ for **1a** and **2a**; $-x + 1$, $y - 1/2$, $-z + 1/2$ for **1b** and **2b**). The intermolecular nearest $Mn\cdots Mn^*$ distance is 9.5943(8) Å for **1a**, 9.8717(6) Å for **1b**, 9.6105-(5) Å for **2a**, and 9.8854(6) Å for **2b** (symmetry operations (*) $-x + 2$, $-y + 1$, $-z + 2$ for **1a** and **2a**; $-x + 1$, $-y + 1$, $-z + 1$ for **1b** and **2b**), and the nearest $M\cdots M^*$ distances are 9.2064(7) Å for **1a**, 9.1917(4) Å for **1b**, 9.3045(3) Å for **2a**, and 9.2847(5) Å for **2b** (symmetry operations (*) $-x + 3/2$, $y - 1/2$, $-z + 3/2$ for **1a** and **2a**; $-x + 1$, $y + 1/2$, $-z + 1/2$ for **1b** and **2b**). Thus, the essential packing arrangements of the tetranuclear complexes are only slightly influenced by the loss of the water molecules.

Magnetic Susceptibility Analysis of 2a and 2b and Determination of Their Spin Ground State. Above 200 K, the susceptibility obeys the Curie–Weiss law with $C = 5.98$ cm³ K mol⁻¹, $\theta = +5.5$ K for **2a** and $C = 5.97$ cm³ K mol⁻¹, $\theta = +9.3$ K for **2b**. The Curie constants correspond well to the spin-only value of 6.0 cm³ K mol⁻¹ with $g = 2.0$ expected for two Mn^{III} ions because of the diamagnetic nature of the square-planar Ni^{II} centers (see structural section). The χT versus T plots for **2a** and **2b** are shown in Figure 4a and Figure S3, respectively. As shown by these figures, the global

magnetic behaviors of **2a** and **2b** are essentially identical. The χT product, 6.11 cm³ K mol⁻¹ for **2a** and 6.16 cm³ K mol⁻¹ for **2b** at 300 K, gradually increases with decreasing temperature to reach a maximum of 8.70 cm³ K mol⁻¹ for **2a** and 9.28 cm³ K mol⁻¹ for **2b** at 6.50 K. At lower temperatures, χT decreases to 7.23 cm³ K mol⁻¹ for **2a** and 7.96 cm³ K mol⁻¹ for **2b** at 1.82 K. As expected from the diamagnetic nature of the Ni^{II} ions, this magnetic behavior is typical for $[Mn_2(saltmen)_2(L)_2]^{2+}$ dinuclear complexes exhibiting $Mn^{III}\cdots Mn^{III}$ ferromagnetic interaction (J_{Mn-Mn}) and anisotropy (ZFS) induced by Mn^{III} ion (D_{Mn}).[6,9,17] Therefore, the magnetic susceptibility can be interpreted by taking into account only a Mn^{III} dinuclear unit and using the spin Hamiltonian

$$H = -2J_{Mn-Mn}\mathbf{S}_{Mn,1}\mathbf{S}_{Mn,2} + 2D_{Mn}S_{Mn,z}^{2} \qquad (1)$$

where $S_{Mn,z}$ is the z component of the $\mathbf{S}_{Mn,i}$ spin vectors. Intercomplex magnetic interaction (zJ') was introduced in the frame of the mean-field approximation to simulate adequately the experimental data.[18] The best simulation is given by a red line in Figure 4a for **2a** (in Figure S3 for **2b**) with corresponding parameters listed in Table 3. The magnitude of these parameters (J_{Mn-Mn}, g, and D_{Mn}) is consistent with the values deduced for **1a** and **1b** (vide infra) and similar to those reported for related Mn^{III} dinuclear complexes.[6,9,17] The reduction of the zJ' value after solvent-elimination is caused by the increase of intermolecular distances as characteristically seen in the intermolecular nearest $Mn\cdots Mn^*$ distance (see structural part). This trend can also be found in the case of **2a** and **2b** (vide infra). From the obtained J_{Mn-Mn} and D_{Mn}, the energy diagram of the two lowest states has been calculated as shown in Figure 4b for **2a** and **2b**. Hence, as well as $[Mn_2(saltmen)_2(ReO_4)_2]$,[6] these compounds possess an $S_T = 4$ ground state and the first excited-state with $S = 3$ that is situated for these compounds at 1.6 K above in energy (considering the shortest energy difference between m_S levels of the two states, $m_S = \pm 1$ for $S_T = 4$ and $m_S = 0$ for $S = 3$). It is worth mentioning that the $S_T = 4$ ground state possesses a nonparabolic shape with spin admixing induced by both isotropic exchange and uni-axial anisotropic terms that have the same order of magni-tude. On the basis of the shape of the ground state seen Figure 4b, the energy to thermally reverse the spin of this system is here the difference of energy between $E(m_S = \pm 4)$ and $E(m_S = \pm 1)$ estimated at $\Delta/k_B = 21.3$ K. In the situation where $J_{Mn-Mn} \gg D_{Mn}$, the estimation of the ground state anisotropy ($D_{ST=4}$) can be easily obtained by the well-known relation: $\Delta = |D_{ST}|S_T^2$ with $D_{ST} = 3D_{Mn}/7$.[19] In this limit and taking $D_{Mn}/k_B = -3.6$ K, D_{ST} and Δ would be equal to -1.5 and 24.7 K. Hence for **2a** and **2b**, the spin mixing induces a slight reduction of the energy barrier.

(17) Lü, Z.; Yuan, M.; Pan, F.; Gao, S.; Zhang, D.; Zhu, D. *Inorg. Chem.* **2006**, *45*, 3538.

(18) The susceptibility was simulated using the MAGPACK package developed by Clemente-Juan et al: Borrás-Almenar, J. J.; Clemente-Juan, J. M.; Coronado, E.; Tsukerblat, B. S. *J. Comput. Chem.* **2001**, *22*, 985.

(19) Boca, R. *Coord. Chem. Rev.* **2004**, *248*, 757.

Table 3. Magnetic Parameters of **1a**, **1b**, **2a**, and **2b** and Related Compounds Containing the Out-of-Plane Mn(III) Dimeric Core (ns = Non-SMM above 1.8 K)[a]

	g	J_{Mn-M} (K)	J_{Mn-Mn} (K)	zJ' (K)	D_{Mn} (K)[b]	D_{ST} (K)[c]	S_T	$\|D_{ST}\|S_T^2$ (K)	τ_0 (s)[d]	Δ_{eff} (K)[d]	ref
I	2.04(1)	−23.7(2)	+0.90(5)	−0.23(2)		~3	2	~12	ns	ns	7
II	2.04(1)	−26.1(2)	+0.70(5)	−0.20(2)		~3	2	~12	ns	ns	7
III	2.04(1)	−25.1(2)	+0.80(5)	−0.23(2)		~3	2	~12	ns	ns	7
IV	1.96(1)	−24.4(2)	+0.40(5)	−0.18(2)		~3	2	~12	ns	ns	7
1a	1.994(2)	−16.0(2)	+1.7(1)	−0.072(2)	−3.6(1)	−1.96(1)	3	17.6			this work
1b	2.032(2)	−14.7(2)	+2.8(1)	−0.023(2)	−3.0(1)	−1.92(1)	3	17.3			this work
V	1.95(1)	−23.0(5)	+2.0(1)	−0.23(2)		−2.1	3	18.9			5
2a	1.995(5)		+1.6(1)	−0.031(2)	−3.6(1)	−1.38(1)	4	22.1	2.5×10^{-7}	13.0	this work
2b	2.05(2)		+1.6(1)	−0.024(2)	−3.6(1)	−1.52(1)	4	24.3	6.2×10^{-7}	10.5	this work
VI	2.00(1)		+2.57	~−0.2	−3.6	−1.63	4	25.5	8×10^{-9}	16	6
VII	1.98		+1.94	0	−2.73	−1.48	4	23.7			17
VIII	1.98		+0.86	0	−1.44	−1.42	4	22.7		17	17

[a] **I**, [Mn₂(saltmen)₂Ni(pao)(bpy)₂](ClO₄)₂; **II**, [Mn₂(5-Clsaltmen)₂Ni(pao)(bpy)₂](ClO₄)₂; **III**, [Mn₂(5-Brsaltmen)₂Ni(pao)(bpy)₂](ClO₄)₂; **IV**, [Mn₂(5-MeOsaltmen)₂Ni(pao)(bpy)₂](ClO₄)₂; **V**, [Mn₂(5-MeOsaltmen)₂(DCNNQI)₂]·MeOH; **VI**, [Mn₂(saltmen)₂(ReO₄)₂]; **VII**, [Mn₂(saltmen)₂(O₂CCH₃)₂]; **VIII**, [Mn₂(saltmen)₂(N₃)₂]. [b] The value was obtained by the χT simulation taking into account zero-field splitting of single Mn^{III} ion. For the blank, such a treatment was not performed in the work. [c] The value was obtained by the M−H simulation for the S_T species. [d] The values were obtained from Arrhenius equation of $\tau(T) = \tau_0 \exp(\Delta_{eff}/k_B T)$. For the blank, exact experimental values have not been given in the literature. Compounds **I**−**IV** did not exhibit any χ'' signal above 1.8 K (see ref 7).

Magnetic Susceptibility Analysis of 1a and 1b and Determination of Their Spin Ground State. For **1a** and **1b**, the susceptibility obeys the Curie−Weiss law above 200 K with $C = 6.69$ cm³ K mol⁻¹, $\theta = -9.1$ K, for **1a** and $C = 6.83$ cm³ K mol⁻¹, $\theta = -1.2$ K, for **1b**. The obtained Curie constants are in good agreement with the expected spin-only value of 6.75 cm³ K mol⁻¹ for two Mn^{III} ions and two Cu^{II} ions with an average g value of 2.0. The negative Weiss constant reveals that the dominant exchange coupling between the spin carriers is antiferromagnetic. It should be first noted that the magnetic behavior observed is essentially identical for both solvated (**a**) and desolvated (**b**) materials. The plot of χT versus T for **1a** is shown in Figure 5a (Figure S4a for **1b**). For **1a** and **1b**, the χT value gradually decreases from 300 K (6.51 cm³ K mol⁻¹ for **1a**, 6.80 cm³ K mol⁻¹ for **1b**) to a minimum at about 22 K (4.78 cm³ K mol⁻¹ for **1a**, 5.59 cm³ K mol⁻¹ for **1b**) and then increases to reach a maximum at 7.8 K for **1a** and 8.0 K for **1b** (5.09 cm³ K mol⁻¹ for **1a**, 5.83 cm³ K mol⁻¹ for **1b**), followed by a decrease to 1.82 K (3.95 cm³ K mol⁻¹ for **1a**, 4.71 cm³ K mol⁻¹ for **1b**). This χT versus T feature is similar to the one observed for the related compounds with [Ni^{II}−NO−Mn^{III}−(O$_{Ph}$)₂−Mn^{III}−ON−Ni^{II}][7] and [Rad−Mn^{III}−(O$_{Ph}$)₂−Mn^{III}−Rad][5] cores. Therefore, as previously observed, the interactions between the Cu^{II} and Mn^{III} ions via the −NO− linkage and between the Mn^{III} ions via the −(O$_{Ph}$)₂− linkage should be strongly antiferromagnetic (J_{Mn-Cu}) and weakly ferromagnetic (J_{Mn-Mn}), respectively. Indeed, the latter contribution is well-known in out-of-plane [Mn₂(5-Rsaltmen)₂(L)₂]$^{0/2+}$ dimers (L = solvent molecules, monodentate ligands).[5,6,7,9] Thus, the magnetic susceptibility of **1a** and **1b** was simulated using the Heisenberg spin Hamiltonian for a linear tetramer system $S_{Cu,1}-S_{Mn,1}-S_{Mn,2}-S_{Cu,2}$ with $S_{Cu,1} = S_{Cu,2} = 1/2$ and $S_{Mn,1} = S_{Mn,2} = 2$

$$H = -2J_{Mn-Mn}\mathbf{S}_{Mn,1}\mathbf{S}_{Mn,2} - $$
$$2J_{Cu-Mn}(\mathbf{S}_{Mn,1}\mathbf{S}_{Cu,1} + \mathbf{S}_{Mn,2}\mathbf{S}_{Cu,2}) + 2D_{Mn}S_{Mn,z}^2 \quad (2)$$

where D_{Mn} is the zero-field splitting (ZFS) parameter of single Mn^{III} ion and $S_{Mn,z}$ is the z component of the S_{Mn} spin
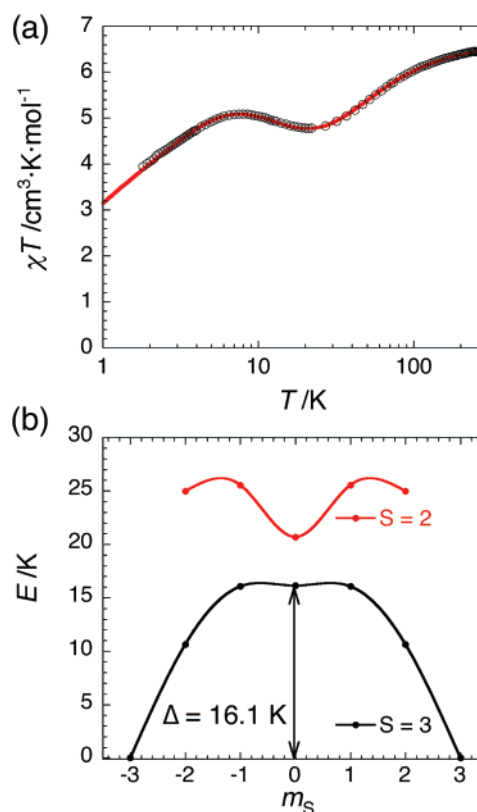

Figure 5. (a) Plots of χT vs T for **1a** at 1 kOe. The solid red line represents best-fit curve with a tetranuclear Cu^{II}−Mn^{III}−Mn^{III}−Cu^{II} model (see text). (b) Energy diagram of the two lowest spin states calculated from the fitting parameters of the χT vs T data. Note that only the dominant spin contribution for each state was kept to make this figure.

vectors. To obtain satisfactory simulations of the experimental data (red lines in Figure 5a for **1a** and Figure S4a for **1b**), the intertetramer interactions (zJ') were taken into account in the frame of the mean-field approximation.[18] The obtained parameters, J_{Cu-Mn}, J_{Mn-Mn}, D_{Mn}, g, and zJ', are listed in Table 3. The antiferromagnetic exchange between the Mn^{III} and Cu^{II} ions via the −NO− bridge is consistent with the previously reported compounds possessing the Cu^{II}−NO−Mn^{III} linkage ($J_{Cu-Mn}/k_B \approx -100$ K in a Cu^{II}−(NO)₃−

Mn^{III} bridging form).[20] Moreover, the values of J_{Mn-Mn} and D_{Mn} fall well in the range of those found in related complexes like **2a** and **2b** (vide supra) and in the family of [Mn$_2$(salt-men)$_2$(L)$_2$]$^{0/2+}$ dimers.[5,6,7,9] It is worth noting that the loss of interstitial solvent in this system seems to have slightly reduced the local anisotropy ($|D_{ST}|/k_B = 3.6$ K → 3 K) and increased J_{Mn-Mn} (1.7 K → 2.8 K). This trend is probably associated with the geometrical changes in the Mn$^{III}_2$ core of the complexes (vide supra). Considering the found parameters, J_{Cu-Mn}, J_{Mn-Mn}, and D_{Mn}, the energy diagrams of the two lowest states can be calculated as shown in Figure 5b for **1a** and Figure S4b for **1b**. From these calculations, both **1a** and **1b** possess an $S_T = 3$ ground state with the $S = 2$ first excited-state at 4.4 and 15.8 K above in energy for **1a** and **1b**, respectively (considering the shortest energy difference between the $m_S = 0$ levels of the $S_T = 3$ and $S = 2$ states). As seen in Figure 5b and discussed above for **2a** and **2b**, the spin mixing is less marked for **1b** than for **1a**, as expected when the ratio J_{Mn-Mn}/D_{Mn} increases. From the obtained energy diagram, the thermal barrier to reverse the spin of these systems is the difference of energy between $E(m_S = \pm 3)$ and $E(m_S = 0)$ estimated at $\Delta/k_B \approx 16.1$ and 15.5 K for **1a** and **1b**, respectively.

Reduced Magnetization and Estimation of the Anisotropy Parameter. The magnetization of the four compounds was measured in the temperature range of 1.8−4.5 K under external fields of 1−7 T. The obtained magnetizations were plotted as a function of H/T in Figure 6 for **1a** and **1b** and Figure 7 for **2a** and **2b**. In the limit where the S_T ground state of a complex is the only thermally populated and in the absence of anisotropic contribution, the isofield magnetization curves should be superimposed and the magnetization (M) would saturate at $M_{sat} = Ng\mu_B S_T$. In the same limit, the non-superimposition of these plots indicates the presence of magnetic anisotropy, consistent with the susceptibility simulations (vide supra). Using the macro-spin approximation and thus the Hamiltonian $H = D_{ST}S_{T,z}^2 + g\mu_B S_T H$, the data have been fitted with a magnetization fitting program "axfit"[21] assuming the respective spin ground states of $S_T = 3$ for **1a** and **1b** and $S_T = 4$ for **2a** and **2b** (Figures 6 and 7). The obtained parameters are $g = 1.87$, $D_{ST=3}/k_B = -1.96$ K for **1a**, $g = 1.95$, $D_{ST=3}/k_B = -1.92$ K for **1b** and $g = 1.90$, $D_{ST=4}/k_B = -1.38$ K for **2a** and $g = 2.00$, $D_{ST=4}/k_B = -1.52$ K for **2b**.

It is worth noting that these D_{ST} parameters lead to energy barriers (calculated in the $J_{Mn-Mn} \gg D_{Mn}$ limit, $\Delta = |D_{ST}|S_T^2$, $\Delta/k_B = 17.6$ K for **1a**, $\Delta/k_B = 17.3$ K for **1b**, $\Delta/k_B = 22.1$ K for **2a** and $\Delta/k_B = 24.3$ K for **2b**) in good agreement with the values evaluated from the energy diagrams shown in Figures 4b, S4b, and 5b. Furthermore, the D_{ST} values are also comparable to those obtained for related SMM com-
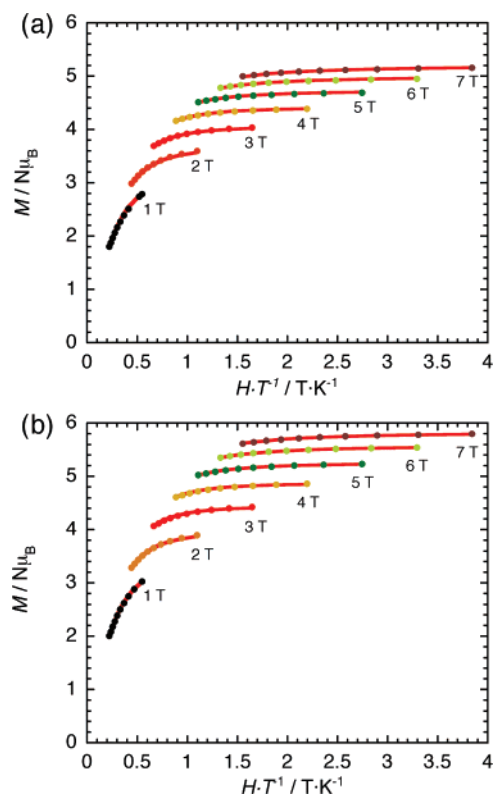
(20) (a) Birkelbach, F.; Flörke, U.; Haupt, H.-J.; Butzlaff, C.; Trautwein, A. X.; Wieghardt, K.; Chaudhuri, P. *Inorg. Chem.* **1998**, *37*, 2000. (b) Birkelbach, F.; Weyhermüller, T.; Lengen, M.; Gerdan, M.; Trautwein, A. X.; Wieghardt, K.; Chaudhuri, P. *J. Chem. Soc., Dalton Trans.* **1997**, 4529.
(21) Yoo, J.; Yamaguchi, A.; Nakano, M.; Krzystek, J.; Streib, W. E.; Brunel, L. C.; Ishimoto, H.; Christou, G.; Hendrickson, D. N. *Inorg. Chem.* **2001**, *40*, 4604.

Figure 6. Plots of M vs H/T for **1a** (a) and **1b** (b). The solid red lines are simulated curves (see text).
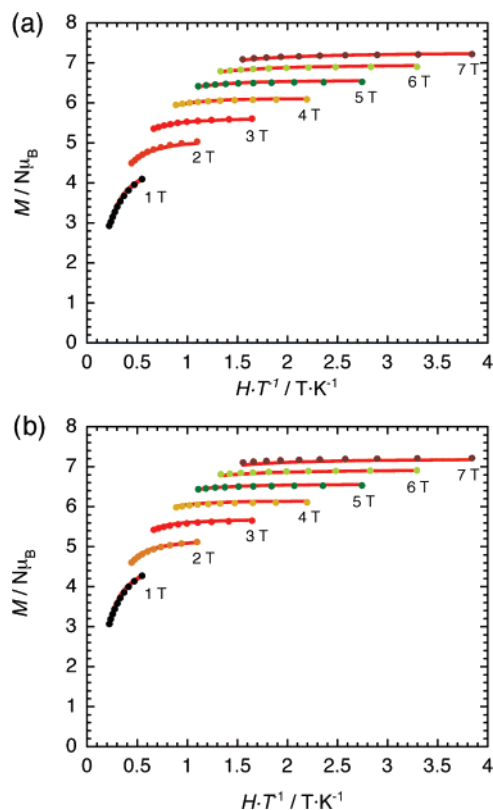
Figure 7. Plots of M vs H/T for **2a** (a) and **2b** (b). The solid red lines are simulated curves (see text).

pounds such as $D_{ST=3}/k_B = -2.1$ K for [Mn$_2$(5-MeOsaltmen)$_2$(DCNNQI)$_2$]·MeOH with $S_T = 3$[5] and $D_{ST=4}/k_B = -1.59$ K for [Mn$_2$(saltmen)$_2$(ReO$_4$)$_2$] with $S_T = 4$.[6] Thus, the similarity
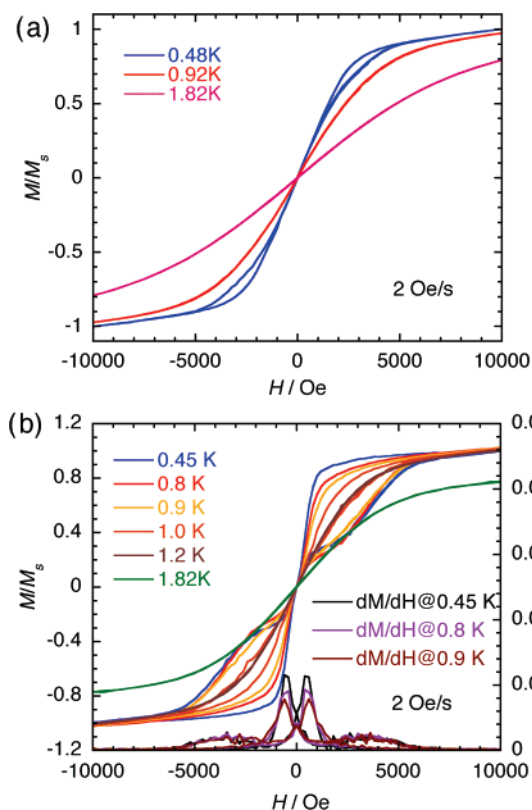
Figure 8. Field dependence of the magnetization on a single crystal of **1a** (a) and **2a** (b) using a commercial SQUID magnetometer attaching a ³He cryostat, where the external field was applied in between the two Jahn–Teller directions of the two complex orientations.

Figure 9. Frequency dependence of the real (χ') and imaginary (χ'') parts of ac susceptibility of **1a** measured at several temperatures under zero dc field and 3 Oe ac field (a) and the dc field dependence of χ'' at 1.82 K (b). The solid lines are guide for the eyes.

of the magnetic parameters between the present compounds and the previously reported SMMs strongly suggests that these four new compounds should behave as SMMs. Therefore, this type of property has been probed using field dependence of the magnetization below 1.8 K and ac susceptibility measurements.

Low-Temperature Magnetic Properties: Evidence of Magnetization Slow Relaxation. Because of the extreme similarity of the magnetic properties between the solvated and desolvated compounds, the whole set of measurements has been done only on **1a** and **2a**. Nevertheless, selected key measurements have been also done on **1b** and **2b** to confirm their quasi-identical behavior. Figure 8 shows field dependence of the magnetization measured below 1.8 K on single crystals of **1a** and **2a** using a commercial SQUID magnetometer equipped with a ³He cryostat. For this measurement, the external field was applied between the two molecular orientations defined by the Jahn–Teller axis of the complexes. For **1a** (Figure 8a), a smooth butterfly type hysteresis loop is observed at 0.48 K, albeit small, suggesting SMM behavior or phonon bottleneck effect.[22–24] This hysteresis is no longer detected at higher temperature as seen on the data at 0.92 K. In contrast, for **2a** (Figure 8b), more
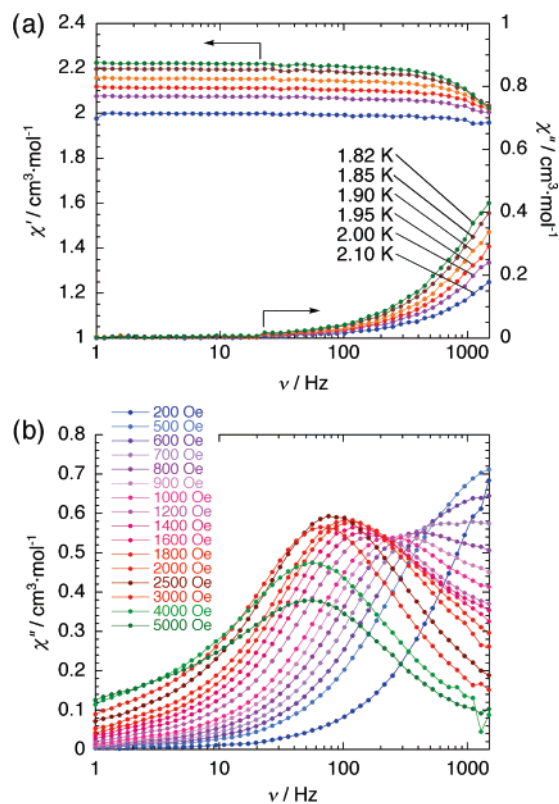
typical hysteresis loops with several step anomalies are observed below 1.0 K. The magnetization passes through zero dc field without coercivity even at 0.45 K. A similar hysteresis feature has been shown in the $S_T = 4$ [Mn₂-(saltmen)₂(ReO₄)₂] SMM.[6] It is interesting to note that the central step of the hysteresis (associated with the ground state QTM) is shifted toward ± 590 Oe, while it should be in zero field for isolated SMMs. Thus, this anomaly confirms the presence of weak intermolecular antiferromagnetic interactions already discussed in the above susceptibility simulation. An estimation of these interactions (zJ'/k_B) can be done at −0.020 K considering $H_{ex} = 590$ Oe and using a relationship of $g\mu_B H_{ex} S_T \cos(\alpha/2) = 2|zJ'|S_T^2 \cos(\alpha)$ (where α is the angle between the two complex orientations, $\alpha = 65°$).[25] It is worth noting that the above estimation is well consistent with the value obtained by the susceptibility simulation.

Slow Relaxation of the Magnetization: ac Susceptibility Measurements. The magnetization relaxation has been studied using ac susceptibility measurements on polycrystalline samples of the four new compounds at several dc fields with an oscillating 3 Oe ac field as a function of frequency (1–1488 Hz) and temperature (1.82–5 K). The in-phase (χ') and out-of-phase (χ'') ac susceptibilities at zero dc field are shown in Figure 9a for **1a** and Figure 10a for **2a** (the desolvated compounds **1b** (Figure S5) and **2b** (Figure

(22) Schenker, R.; Leuenberger, M. N.; Chaboussant, G.; Güdel, H. U.; Loss, D. *Chem. Phys. Lett.* **2002**, *358*, 413.
(23) Rumberger, E. M.; Hill, S.; Edwards, R. S.; Wernsdorfer, W.; Zakharov, L. N.; Rheingold, A. L.; Christou, G.; Hendrickson, D. N. *Polyhedron* **2003**, *22*, 1865.
(24) Chiorescu, I.; Wernsdorfer, W.; Müller, A.; Bögge, H.; Barbara, B. *Phys. Rev. Lett.* **2000**, *84*, 3454.

(25) Herpin, A. Théorie du magnétisme. In *Bibliotheque des Sciences et Techniques Nucleaires;* Presses Universite de France: Paris, 1968.
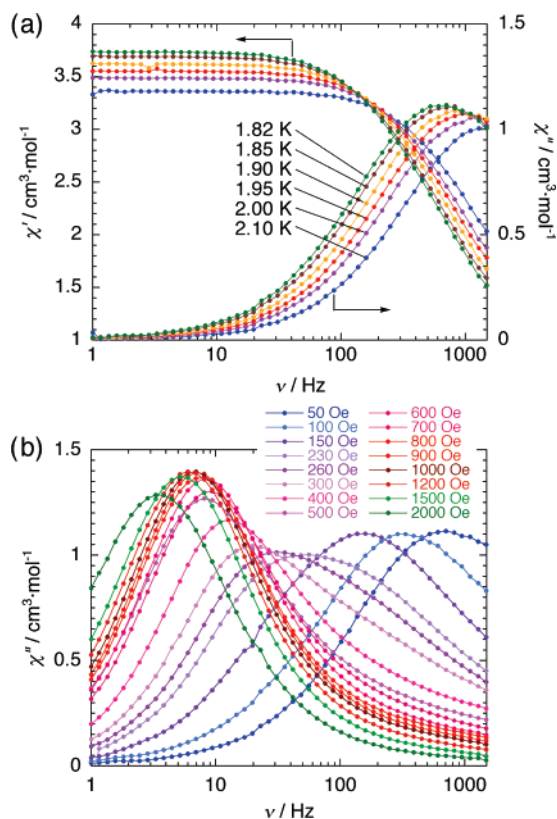
Figure 10. Frequency dependence of the real (χ') and imaginary (χ'') parts of ac susceptibility of **2a** measured at several temperatures under zero dc field and 3 Oe ac field (a) and the dc field dependence of χ'' at 1. 82 K (b). The solid lines are only guide for the eyes.

Figure 11. dc field dependence of the relaxation time (τ) at 1.82 K (blue line) and energy barrier (Δ) derived from the Arrhenius relation $\tau = \tau_0 \cdot \exp(\Delta/k_B T)$ (red line) for **1a** (a) and **2a** (b). The solid lines are only guide for the eyes.

S6) exhibit very similar behavior to that of **1a** and **2a**, respectively). For both series of **1** and **2**, χ' and χ'' are frequency dependent, indicating the possibility of SMM behavior despite the absence of clear χ'' peaks (i.e., relaxation mode) for **1a** and **1b** above 1.8 K. It is interesting to note that the slow relaxation of the magnetization occurs at higher temperatures for **2** than for **1**, this result being at least partially associated with the respective value of the spin ground state: $S_T = 4$ for **2** and $S_T = 3$ for **1**. For **2a** and **2b**, the relaxation times deduced from the maximum of the out-of-phase ac susceptibility obey a thermally activated Arrhenius relation with $\tau_0 = 2.5 \times 10^{-7}$ s, $\Delta_{eff}/k_B = 13$ K for **2a** and $\tau_0 = 6.2 \times 10^{-7}$ s, $\Delta_{eff}/k_B = 10.5$ K for **2b** (their Arrhenius plots are shown in Figure S7). This effective energy barrier is significantly smaller than the expected values estimated by the susceptibility simulation or reduced magnetization fits ($\Delta/k_B \approx 21-24$ K for **2**). As observed in many SMMs, it is likely that the observed Δ_{eff} take an effective value, resulting from a "short-cut" of the thermal barrier by QTM. This second path of relaxation is indeed clearly dominant at low temperatures as shown by the hysteresis loops display in Figure 8. At higher temperatures, the QTM pathway is not anymore dominant but can still influence the thermal relaxation of the magnetization. Therefore, to confirm the presence of QTM, additional ac susceptibility measurements have been performed under small magnetic fields that could remove the degeneracy of the m_S states and thus possible zero-field quantum tunneling between the $\pm m_S$ states. Figures 9b and 10b show the dc
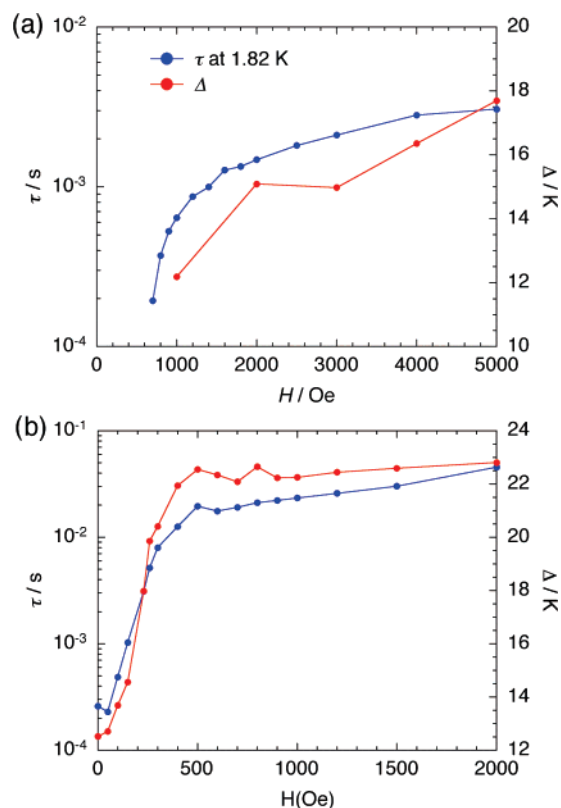
field dependence of χ'' measured at 1.82 K for **1a** and **2a**, respectively. In both compounds, the χ'' peak shifts to low frequency with increasing dc field. The characteristic relaxation times (τ) estimated from out-of phase susceptibility peaks and the characteristic energy barriers (Δ) have been plotted as a function of dc field in Figure 11 (blue dots and line, the relaxation time at 1.82 K; red dots and line, the energy barrier). The relaxation time that reaches nearly 10^{-4} s at low dc field for **1a** and of 3×10^{-4} s at zero field for **2a**, becomes rapidly slower when dc field is applied up to 2000 Oe for **1a** and 500 Oe for **2a** and then tends to saturate at higher fields to $\sim 3 \times 10^{-3}$ s and $\sim 3 \times 10^{-2}$ s for **1a** and **2a**, respectively. Therefore, as expected when a fast relaxation pathway is suppressed, the relaxation time of the systems becomes longer and dominates by the thermal relaxation. The energy barrier exhibits also a quasisaturation under moderated fields: 16.5 and 15.0 K under 4000 Oe for **1a** and **1b,** respectively, and 22.6 and 21.8 K under 500 Oe for **2a** and **2b,** respectively (Figure S7). As anticipated, these values are in good agreement with the values deduced from the energy diagrams ($\Delta/k_B = 16.1$ and 21.3 K for **1a** and **2a**, respectively, Figures 4, 5, and S3) and are consistent with the values deduced from the fit of reduced magnetization ($\Delta/k_B = 17.6$ K for **1a** and 22.1 K for **2a,** Figures 6 and 7). Consequently these results indicate that the reduction of the energy barrier (Δ_{eff}) under zero dc field is probably induced QTM. These dynamic behaviors strongly support that **1** and **2** are both SMMs with intrinsic characteristics quasi-independent of their solvation.

Conclusions

We have shown in this work that it was possible to chemically tune the SMM properties of targeted hetero-metallic tetranuclear complexes by modification of the decorating additional metal building unit (based on Cu^{II} or Ni^{II}) without change of the Mn^{III} dinuclear core. This result has been investigated in a couple of isostructural compounds: **1a** and **2a** and their dried versions **1b** and **2b**, for which the crystal structure and magnetism remain essentially ones of the respective parent compounds. Compound **1a** and **1b** with $M^{II} = Cu^{II}$ possesses an $S_T = 3$ ground state induced by a combination of antiferromagnetic exchange between the Mn^{III} and Cu^{II} ions and ferromagnetic exchange between the Mn^{III} ions. The presence of uniaxial anisotropy generates an energy barrier for the magnetization reversal around 16 K. In contrast, compounds **2a** and **2b** with $M^{II} = Ni^{II}$ possess an $S_T = 4$ ground state because of the ferromagnetic coupling in the Mn^{III} dimeric moiety (the Ni^{II} unit being diamagnetic). Again, uniaxial anisotropy induced by the Mn^{III} ions creates an energy barrier on the ground state of about 22 K. These examples illustrate how the SMM properties can be controlled using chemical modification of a known system. This chemically flexibility is one of the most important advantages found in the bottom-up approach to design nanosized magnetic materials. However, such examples are still rare as shown in the introduction section. In the present compounds, one kind of coordination-donor building blocks, but containing different metal ions of either Cu^{II} or Ni^{II}, has been used to decorate the Mn^{III} dimeric SMM core acting as a coordination-acceptor building block to synthesize new heterometallic complexes. This synthetic strategy has allowed us to tune the magnetic properties of an invariable SMM core by choosing the terminal metal ion and bridging groups.[5−7] In the same lines, networks of different dimen-sionalities based on the same dinuclear Mn^{III} unit should be obtained by using multidentate coordination-donor building blocks as already exemplified by the rational design of single-chain magnet systems.[26]

Supporting Information Available: Crystallographic data in CIF format for **1a**, **1b**, **2a**, and **2b** and Figures S1−S7. This material is available free of charge via the Internet at http://pubs.acs.org. Data have been deposited as CIFs at the Cambridge Data Centre as supplementary publications CCDC-626226 for **1a**, CCDC-626227 for **1b**, CCDC-626228 for **2a**, and CCDC-626229 for **2b**. Copies of the data can be obtained free of charge on application to CCDC, 12 Union Road, Cambridge CB21EZ, UK (fax (+44) 1223−336-033; e-mail deposit@ccdc.cam.ac.uk).

IC0620891

(26) (a) Clérac, R.; Miyasaka, H.; Yamashita, M.; Coulon, C. *J. Am. Chem. Soc.* **2002**, *124*, 12837. (b) Miyasaka, H.; Clérac, R.; Mizushima, K.; Sugiura, K.; Yamashita, M.; Wernsdorfer, W.; Coulon, C. *Inorg. Chem.* **2003**, *42*, 8203. (c) Ferbinteanu, M.; Miyasaka, H.; Wernsdorfer, W.; Nakata, K.; Sugiura, K.; Yamashita, M.; Coulon, C.; Clérac, R. *J. Am. Chem. Soc.* **2005**, *127*, 3090−3099. (d) Miyasaka, H.; Madanbashi, T.; Sugimoto, K.; Nakazawa, Y.; Wernsdorfer, W.; Sugiura, K.; Yamashita, M.; Coulon, C.; Clérac, R. *Chem.−Eur. J.* **2006**, *12*, 7028. (e) Saitoh, A.; Miyasaka, H.; Yamashita, M.; Clérac, R. *J. Mater. Chem.* **2007**, *17*, 2002.